symmetry

MDPI

Article

Generalized MGT Heat Transfer Model for an Electro-Thermal Microbeam Lying on a Viscous-Pasternak Foundation with a Laser Excitation Heat Source

Ahmed E. Abouelregal [1,*], Marin Marin [2] and Sameh S. Askar [3]

1 Department of Mathematics, Faculty of Science, Mansoura University, Mansoura 35516, Egypt
2 Department of Mathematics and Computer Science, Transilvania University of Brasov, 500036 Brasov, Romania; m.marin@unitbv.ro
3 Department of Statistics and Operations Research, College of Science, King Saud University, P.O. Box 2455, Riyadh 11451, Saudi Arabia
* Correspondence: ahabogal@gmail.com

Abstract: In this study, the effects of laser light on the heat transfer of a thin beam heated by an applied current and voltage are investigated. Laser heating pulses are simulated as endogenous heat sources with discrete temporal properties. The heat conduction equation is developed using the energy conservation equation and the modified Moore–Gibson–Thompson (MGT) heat flow vector. Thermal and structural analysis of Euler–Bernoulli microbeams is provided with the support of visco-Pasternak's base with three parameters. Using the Laplace transform method, an approximation of an analytical solution is found for the field variables being examined. A comparison was made of the impacts of laser pulse length, the three foundation coefficients, and the thermal parameters on the responses to changes in measured thermophysical fields, such as deflection and temperature.

Keywords: Winkler–Pasternak foundation; microbeams; laser heating; MGT model

Citation: Abouelregal, A.E.; Marin, M.; Askar, S.S. Generalized MGT Heat Transfer Model for an Electro-Thermal Microbeam Lying on a Viscous-Pasternak Foundation with a Laser Excitation Heat Source. *Symmetry* **2023**, *15*, 814. https://doi.org/10.3390/sym15040814

Academic Editor: Mariano Torrisi

Received: 13 February 2023
Revised: 15 March 2023
Accepted: 24 March 2023
Published: 27 March 2023

1. Introduction

The principles of the theory of elasticity lead to inherent symmetries in the associated elasticity tensor, which defines any linearly elastic continuum at a given position. Furthermore, an elasticity tensor may display additional context-specific symmetries. This study focuses on these later symmetries, sometimes known as "material symmetries". When symmetry is involved, it can be found in the bifurcation theory, physics, and the mechanics of materials when constituent tensors, such as the elastic tensor, require classification. Moreover, several formulas for coordination-free criteria for determining elastic tensors with a given symmetry class can be found in the literature, complementing experimental and numerical techniques.

There are always new developments in nanoelectromechanical systems research and development. Mechanical devices are becoming thinner and narrower to lessen their mass, raise their resonance frequency, and decrease their force constants. Improvements in manufacturing procedures and the development of novel techniques for actuating and sensing nanoscale motion are examples of recent developments in this area [1]. Microelectromechanical systems (MEMS) are one of the most critical technologies of the 21st century. It combines silicon-based microelectronics and micro industry, two of the most advanced technologies. Its microsystem-based methods and technologies may improve the overall quality of human life.

Because MEMS is a combination of many different fields, its design, construction, and manufacturing depend on mechanical design, solid-state physics, microelectronics, biological sciences, chemical engineering, hydrodynamic engineering, optical devices, sensor systems, and packaging. The variety of industries and uses that employ MEMS indicates its sophistication. Accelerometers for airbag sensors are one example of an MEMS device that is made and used commercially [2]. In today's world, microelectromechanical systems can be found in everything from automobiles to healthcare, electronics, communications, and even military systems. Li et al. [3] studied the nonlinear in-plane instability of shallow circular arches made of functionally graded carbon nanotube-reinforced composite that were limited by rotational symmetry and put under constant radial stress in a temperature environment. Li [4] is also interested in the transverse vibrations of axially moving nanobeams. This is in addition to the effects of the strain gradient and temperature. It considers the thermal behavior and the concept of strain gradient elasticity. Li et al. [5] investigated the motion of a piezoelectric nanoribbon under the influence of thermomechanical and electrical forces. This is employed as a model for the intrinsic component of medical nanorobotics. Sui et al. [6] described the vibrational properties of axially moving, fairly thick plates supported by an elastic base. The plate is made of functionally graded (FG) materials, and both its dynamic and kinematic conditions including the vibration's inherent frequency and axial velocity are taken into consideration. Zemskov et al. [7] discussed the issue of unstable vibrations in a Bernoulli–Euler beam while considering temperature and diffusion processes that relax with time. The first mathematical model comprises an equation set for the beam's unstable bending vibrations that consider heat transfer and mass transfer.

In civil engineering, rigid road slabs, airport asphalt, tall building foundations, sidewalk platforms, etc., are often made with flexible-based composite structures. In these cases, it is important to consider the mechanical properties of structures mounted on an elastic base, as they are important considerations for design, use, and maintenance. For this reason, one of the most exciting areas of research in this field has been the analysis of the vibration response of laminated slabs and small beams supported by flexible foundations. Based on the literature in this context, there are two main types of flexible baseboard models: the Winkler type and the two-parameter models, such as the Pasternak model [8].

Winkler proposed the first linear foundation. Many papers have been written about this issue, exploring various approaches such as Winkler or Pasternak foundations, flexible or viscoelastic foundations, linear or non-linear assumptions, etc. In contrast to the Pasternak foundation coefficients, which can withstand both normal and transverse shear stresses, the Winkler modulus can only handle normal loads [9]. The two-parameter elastic foundation model is presented as the investigation proceeds further. The discontinuity may be efficiently removed by representing the soil's compressive strength and shear strength with two separate factors, thereby overcoming the shortcomings of the Winkler foundation type. The Pasternak basis is commonly employed in the two-parameter type [10]. Zemskov and Tarlakovskii [11] considered an orthotropic Timoshenko beam with a uniformly distributed transverse load, rests on an elastic base, and is supported by an elastic base. The problem is one of unstable elastic diffusion resonance. On a flexible basis, they employed the Winkler framework. For the theoretical analysis, they employed a set of Timoshenko beam bending formulas that include diffusion. Zemskov et al. [12] studied the issue of unstable vibrations in a simply supported Euler–Bernoulli beam subject to a distributed transverse force. They employ a set of beam deflection formulas with inner diffusion processes to formulate the mathematical issue.

Joule heating is often used as a trigger mechanism in microelectromechanical systems (MEMS) because it is easy to understand. The term "joule heating" refers to the process by which the electrical current of a building is converted into heat energy. In order to regulate the axial tension caused by thermal expansion from within the microbeam, a VTH electrothermal voltage (thermoelectric potential) is introduced between the microbeam stabilizers, causing an ITH current to flow through the beam, but the permanent anchors of the microbeam, which cause a compressive force, prevent any elongation from occurring. The microbeam might buckle (deform) under such compressive stress. There are two ways to approach the study of this mechanism: the thermoelectric case, which explains the conversion of electrical energy into heat, and the thermoelasticity case, which accounts for the conversion of thermal energy into compressive stress [13]. Joule heating is produced when an electric current flows through a conductor and interacts with the moving particles that make up the current and the atomic ions that make up the conductor itself. When these particles, which make up the electric current, collide with an ion, they lose some of their momentum in the process. This kinetic energy makes the conductor's internal temperature rise, which turns the electrical energy into thermal energy [14].

In recent decades, researchers have paid particular attention to innovative, continuous models of deformable materials. It is known that the internal structural motions of matter play an important role in determining how matter interacts with external stimuli. Conventional flexibility completely ignores this effect because it only gives degrees of freedom in translation to physical locations in the body. In thermoelasticity, the interplay between elasticity and heat transfer is analyzed theoretically. Thermal stresses and thermoelastic deformations in a variety of materials have been the focus of a great deal of research in recent decades [15]. Researchers are exploring thermoelasticity because of its usefulness in many different branches of engineering and science. The thermoelastic phenomenon is briefly discussed in light of different computational techniques. When solving heat transfer issues using thermoelasticity theory, the outcomes vary depending on the starting and limiting conditions [16].

Based on Biot's system of mixed parabolic and hyperbolic Biot equations [17], conventional thermodynamic models predict some physical observations and outcomes that contradict physical phenomena. These observations include the infinite velocities of the thermal signals. That is why many researchers have revised the concept of traditional coupled dynamic thermoelasticity in this context to address this problem. The majority of proposals are based on the development of the classic Fourier law of heat transfer. Among these proposed thermal models are those that include periods of thermal relaxation (thermal delay time). In recent years, Lord and Shulman [18], Green and Lindsay [19], and Green and Naghdi [20–22] have published different modified heat transfer models. These systems are the hyperbolic heat equations that have received the most attention in the literature.

From a mathematical and computational point of view, the individual physical phenomena that make up many linked issues are well explained and sophisticated models that can be used to describe their mathematical representation. On the other hand, there are some situations in which a new model is necessary. This is because the current standard concept for discussing certain physical processes has been shown to be insufficient, and it can even sometimes lead to contradictions within some well-established physical systems. In these situations, a new framework is formulated. In this study, the Moore–Gibson–Thompson (MGT) equation will be used to figure out how heat moves in a thermoelastic system. This model emerges due to the insertion of a relaxation parameter into the Green–Naghdi type III framework [23]. Quintanilla [24] presented a thermoelastic model in which the MGT equation includes the heat transfer rate. In this context, Quintanilla [16] also proposed a two-temperature system for the Moore–Gibson–Thompson heat transfer equation. In previous embodiments, Quintanilla has shown that solutions are well-rendered and fade exponentially when the constituent parameters are set correctly. Since the advent of the MGT equation theory of thermoelasticity in the field of fluids, many studies have been conducted on this topic [25–32].

In many engineering applications, optimal design requires performing the elastic thermal vibration analysis of microbeams on an elastic basis. However, no solutions have been developed for the thermoelastic vibration issues that arise when thermal coupling is included in analyses of such structures resting on three-parameter viscoelastic elastic bases. For this purpose, the investigation of how the Winkler and Pasternak foundations affect the thermoelastic behavior of an Euler–Bernoulli beam is proposed. In order to achieve this, it was necessary to solve the derived differential equation that governs this system in order to obtain the distributions of various physical domains. Moreover, the generalized heat transfer equation has been modified based on the MGT equation and is considered the first proposal in this field. Using a three-parameter viscoelastic basis and taking into account the thermoelastic coupling effect, the thermoelastic behaviors of microbeam resonators were studied as a result of the effects of the initial axial tension, the effects of the laser pulse, and the voltage. Finally, the numerical results of the different fields obtained are presented graphically and discussed in detail.

2. Theoretical Analysis and Basic Equations

In the theory of thermoelasticity of homogeneous conductive solids for heat transfer, the following set of governing equations can be written [33]:

$$\sigma_{kl} = 2\mu e_{kl} + (\lambda e_{mm} - \gamma\theta)\delta_{kl}, \tag{1}$$

$$\eta = \frac{\rho C_E}{\rho T_0}\theta + \frac{\gamma}{\rho} e_{kl}, \tag{2}$$

$$2e_{kl} = u_{k,l} + u_{l,k}, \tag{3}$$

$$\rho T_0 \frac{\partial \eta}{\partial t} = -q_{l,l} + \rho Q, \quad l, k = 1, 2, 3. \tag{4}$$

In these equations, ε_{kl} denotes the strain tensor, σ_{kl} is the stress tensor, u_l represents the displacement components, η symbolizes the entropy, q_l denotes the heat flow components, Q signifies the heat source, C_E is the specific heat, δ_{kl} represents the Kronecker delta, and ρ is the material density. The symbols λ and μ are the usual Lame's constants, $\gamma = (3\lambda + 2\mu)\alpha_t$, and α_t is the thermal expansion coefficient. Additionally, $\theta = T - T_0$ is the temperature increment, where T_0 is the reference temperature.

The revised version of Fourier's Law that is in line with the GN-III context [21] may be written as:

$$q_l = -K\theta_{,l} - K^*\vartheta_{,l} \tag{5}$$

where ϑ symbolizes the thermal displacement, K^* refers to the material characteristics, K is the thermal conductivity, and $\vartheta = \int \theta dt$.

The suggested improved heat equation was developed by Quintanilla [15,16] after the relaxation coefficient τ_0 was implemented into the Green–Naghdi framework of type III. Therefore, the resulting revised heat transfer equation will be in the form of [23,24]:

$$\left(1 + \tau_0 \frac{\partial}{\partial t}\right) q_l = -K\theta_{,l} - K^*\vartheta_{,l}. \tag{6}$$

A modified MGT heat transfer equation is obtained by combining Equations (2), (4), and (6) as follows:

$$\left(1 + \tau_0 \frac{\partial}{\partial t}\right)\left[\rho C_E \frac{\partial^2 \theta}{\partial t^2} + T_0\gamma \frac{\partial^2}{\partial t^2}\left(u_{m,m}\right) - \rho\frac{\partial Q}{\partial t}\right] = \left(K\frac{\partial}{\partial t} + K^*\right)\nabla^2\theta \tag{7}$$

3. Model Description

As illustrated in Figure 1, a thin Bernoulli–Euler thermoelastic beam supported by a viscoelastic foundation with three parameters and loaded with a thermoelectric current was considered. The microbeam has an isotropic shape with a constant cross-sectional area, denoted by A, thickness h, and length, denoted by L. It is presumed that a Cartesian coordinate system (x, y, z) is being used, with the origin located on the left side of the beam and in the middle of its thickness. The microbeam is first assumed to be at room temperature T_0, and then it is exposed to a short-pulse laser heating at an absorption rate of $Q(x, z, t)$ of laser energy.

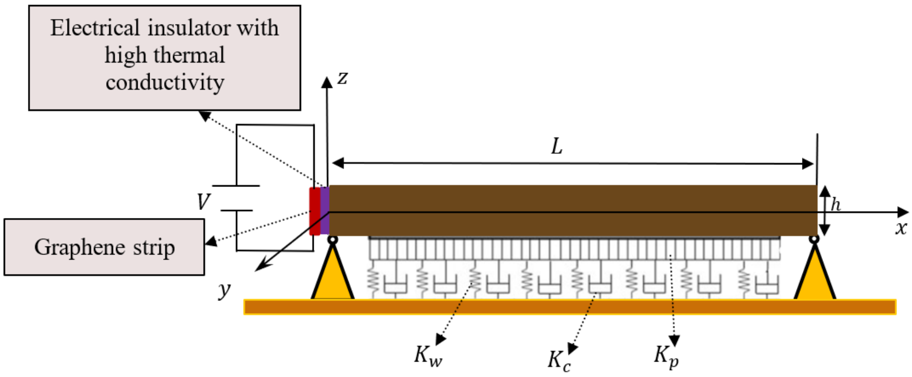

Figure 1. Illustration of a slender beam based on visco-Pasternak's Base.

It is assumed that the beam deflects in a manner consistent with the Euler–Bernoulli model (small deflections $w(x,t)$) as a result of its exposure to bending vibrations of small amplitude around x-axis. If the Euler–Bernoulli beam model is considered, the displacement and strain components can be written as follows:

$$u = -z\frac{\partial w}{\partial x}, \quad v = 0, \quad w(x,y,z,t) = w(x,t), \tag{8}$$

$$e_{xx} = e = z\frac{\partial^2 w}{\partial x^2}. \tag{9}$$

Pasternak's model has been utilized to characterize the soil foundation so that shear contact between the springs may be calculated. To do this, the spring components will be joined to a layer of incompressible vertical elements that are subject only to transverse shear deformation. Because of its relative ease of use, Pasternak's two-parameter system has garnered the most attention from engineers. The impact of the underappreciated shear–strain energy on the soil is taken into consideration in the Pasternak version. Pasternak's basis formula, which is based on transverse displacement, forms an elastic reaction to the foundation and is as follows [33,34]:

$$p(x,t) = K_w w - K_p\frac{\partial^2 w}{\partial x^2} \tag{10}$$

where the Winkler and Pasternak moduli are denoted by the parameters K_w and K_p, respectively.

In order to account for the effects of viscoelasticity, Kelvin–Voigt included them in the elastic Pasternak model. The elastic foundation force can be expressed as [34]:

$$p(x,t) = K_w w - K_p\frac{\partial^2 w}{\partial x^2} + K_v\frac{\partial w}{\partial t} \tag{11}$$

where K_v represents the damping of the foundation caused by the viscous components. In the special situation where K_p is equal to zero, Equation (11) depicts the reaction of the viscoelastic Winkler foundation. If the microbeam is not supported by the elastic basis, then $K_w = K_p = K_0 = 0$, and Equation (11) may be simplified to become that which is described in [35].

For the Bernoulli–Euler microbeam shown in Figure 1, the linear bending issue may be represented by the following equation of motion in terms of the Pasternak's basis, $p(x,t)$, and the bending moment, $M(x,t)$ [36,37]:

$$\frac{\partial^2 M}{\partial x^2} = \rho A\frac{\partial^2 w}{\partial t^2} + p(x,t) \tag{12}$$

It is possible to calculate the Bernoulli–Euler flexural moment of the microbeam using the following equation

$$M = \int z\,\sigma_x \mathrm{d}A \tag{13}$$

where σ_x is the single constitutive connection for a one-dimensional problem, and the expression for this relationship is provided by:

$$\sigma_x = E\frac{\partial u}{\partial x} - \frac{\alpha_t E}{(1-2\nu)}\theta = -Ez\frac{\partial^2 w}{\partial x^2} - \frac{\alpha_t}{(1-2\nu)}E\theta \tag{14}$$

In Equation (14), E, α_t, and ν denote Young's modulus, the coefficient of the thermal expansion, and Poisson's beam ratio, respectively. When (14) is substituted into (13), the flexural moment can be derived as follows:

$$M = -EI\left[\frac{\partial^2 w}{\partial x^2} + \alpha_T M_T\right] \tag{15}$$

where $\alpha_T = \alpha_t/(1-2\nu)$, $I = bh^3/12$ represents the moment of inertia, EI stands for the flexural stiffness of the microbeam, and M_T is the thermal moment described by the expression:

$$M_T = \frac{12}{h^3}\int_{-h/2}^{h/2} \theta(x,z,t) z \mathrm{d}z \tag{16}$$

By plugging Equation (15) into Equation (12), it is possible to derive:

$$\left[EI\frac{\partial^4}{\partial x^4} - K_p\frac{\partial^2}{\partial x^2} + K_w + \rho A\frac{\partial^2}{\partial t^2} + K_v\frac{\partial}{\partial t}\right]w + \alpha_T EI\frac{\partial^2 M_T}{\partial x^2} = 0. \tag{17}$$

When Equations (7) and (8) are used, one can determine the MGT heat transport in terms of temperature θ and transverse displacement w as follows:

$$\begin{aligned}\left(K^* + K\frac{\partial}{\partial t}\right)\left(\frac{\partial^2\theta}{\partial x^2} + \frac{\partial^2\theta}{\partial z^2}\right) + \rho\left(1 + \tau_0\frac{\partial}{\partial t}\right)\frac{\partial Q}{\partial t} \\ = \left(1 + \tau_0\frac{\partial}{\partial t}\right)\frac{\partial^2}{\partial t^2}\left[\rho C_E\theta - (\alpha_T E T_0)z\frac{\partial^2 w}{\partial x^2}\right].\end{aligned} \tag{18}$$

It will be considered that the upper and lower sides of the package are thermally insulated. As a result, we will have $\frac{\partial\theta}{\partial z} = 0$ at $z = \pm h/2$. Additionally, for the current microbeam, it is presumed that the temperature increase varies sinusoidally in the direction of the thickness. Therefore, the following assumption can be taken into account:

$$\theta(x,z,t) = \Theta(x,t)\sin\left(\frac{\pi z}{h}\right) \tag{19}$$

When Equation (19) is substituted into Equations (15) and (17), the resulting equations are:

$$\left[IE\frac{\partial^4}{\partial x^4} - K_p\frac{\partial^2}{\partial x^2} + \rho A\frac{\partial^2}{\partial t^2} + K_v\frac{\partial}{\partial t} + K_w\right]w + \frac{24IE\alpha_T}{h\pi^2}\frac{\partial^2\Theta}{\partial x^2} = 0, \tag{20}$$

$$M = -IE\frac{\partial^2 w}{\partial x^2} - \left(\frac{24IE\alpha_T}{h\pi^2}\right)\Theta \tag{21}$$

Following the multiplication by $\frac{12}{h^3}z$, the integration, together with the microbeam thickness in Equation (18), produces the following results:

$$\begin{aligned}\left(1 + \tau_0\frac{\partial}{\partial t}\right)\frac{\partial^2}{\partial t^2}\left[\frac{\rho C_E}{K}\Theta - \left(\frac{\alpha_T\pi^2 h T_0 E}{24K}\right)\frac{\partial^2 w}{\partial x^2}\right] = \left(K^* + K\frac{\partial}{\partial t}\right)\left(\frac{\partial^2\Theta}{\partial x^2} - \frac{\pi^2}{h^2}\Theta\right) \\ + \left(\frac{\pi^2}{2Kh^2}\right)\left(1 + \tau_0\frac{\partial}{\partial t}\right)\int_{-h/2}^{h/2} z\frac{\partial Q}{\partial t}\mathrm{d}z\,.\end{aligned} \tag{22}$$

4. Solution of the Governing Equations

Normalization must be performed first so that the governing equations can be solved. As a result, the following nondimensional variables can be introduced:

$$\begin{gathered}\Theta' = \frac{\Theta}{T_0}, \quad \sigma_x' = \frac{1}{E}\sigma_x, \{t', \tau_0'\} = \frac{\vartheta^2}{k}\{t, \tau_0\}, \{x', z'\} = \frac{\vartheta}{k}\{x, z\}, K_v' = \frac{\vartheta^2 K_v}{kIE}, \\ M' = \frac{kM}{\vartheta IE}, \{w', u'\} = \frac{\vartheta}{k}\{w, u\}, \qquad Q' = \frac{k^2 Q}{\vartheta^2 K T_0}, K_w' = \frac{1}{IE}K_w, K_p' = \frac{\vartheta^2}{k^2 IE}K_p,\end{gathered} \tag{23}$$

where $\vartheta = \sqrt{\frac{E}{\rho}}$ and $\frac{1}{k} = \frac{\rho C_E}{K}$.

Equations (14) and (20)–(22) can be rewritten after using the above nondimensional parameters (eliminating primes for convenience) as:

$$\left[\frac{\partial^4}{\partial x^4} - K_p\frac{\partial^2}{\partial x^2} + \frac{12}{h^2}\frac{\partial^2}{\partial t^2} + K_v\frac{\partial}{\partial t} + K_w\right]w = -\left(\frac{24\vartheta T_0 \alpha_T}{k\pi^2 h}\right)\frac{\partial^2 \Theta}{\partial x^2} \tag{24}$$

$$\begin{aligned}\left(1 + \tau_0\frac{\partial}{\partial t}\right)\frac{\partial^2}{\partial t^2}\left[\Theta - \left(\frac{\alpha_T \pi^2 T_0^2 h \vartheta E}{24K}\right)\frac{\partial^2 w}{\partial x^2}\right] = \left(\frac{kK^*}{\vartheta^2 K} + \frac{\partial}{\partial t}\right)\left(\frac{\partial^2 \Theta}{\partial x^2} - \frac{\pi^2}{h^2}\Theta\right) \\ - \frac{\pi^2}{2}\left(1 + \tau_0\frac{\partial}{\partial t}\right)\int_{-h/2}^{h/2} z\frac{\partial Q}{\partial t}\mathrm{d}z,\end{aligned} \tag{25}$$

$$M = -\frac{\partial^2 w}{\partial x^2} - \left(\frac{24\vartheta T_0 \alpha_T}{kh\pi^2}\right)\Theta \tag{26}$$

$$\sigma_x = -z\frac{\partial^2 w}{\partial x^2} - (\alpha_T T_0)\theta. \tag{27}$$

The diversity of laser pulses and their distinctive properties in the fabrication and development of elements with complex geometries and the integration of many components into one integrated part have gained significant engineering and scientific interest in recent years. In the surface heat source model $Q(x, z, t)$, the pattern of surface heat flow to the upper surface of the microbeam, which is assumed to follow a Gaussian distribution, is supposed to be of the following form [38,39]:

$$Q(x, z, t) = \sqrt{\frac{4\ln(2)}{\pi}}\left(\frac{1 - R}{dt_p}\right)I_0 e^{\left(-\frac{x}{d}\right)} e^{-\beta\left|\frac{t - 2t_p}{t_p}\right|} \tag{28}$$

where I_0 is the laser fluence (J/m²), d symbolizes the laser penetration depth, t_p denotes the length of time that the laser pulse is active, and the reflectance of the surface denoted by R and β is a constant parameter.

5. Initial and Boundary Conditions

In the beginning, at $t = 0$, the microbeam is taken to be at rest, and the initial circumstances are supposed to be:

$$\begin{gathered}\Theta(x, 0) = 0 = \frac{\partial \Theta(x, 0)}{\partial t}, \quad w(x, 0) = 0 = \frac{\partial w(x, 0)}{\partial t}, \\ u(x, 0) = 0 = \frac{\partial u(x, 0)}{\partial t}, \quad \sigma_x(x, 0) = 0 = \frac{\partial \sigma_x(x, 0)}{\partial t}.\end{gathered} \tag{29}$$

Boundary conditions are necessary to ensure the possibility of a complete solution to the system of differential equations. In this work, the following mechanical boundary conditions will be taken into account

$$w(x,t)=0,\quad \frac{\partial^2 w(x,t)}{\partial x^2}=0,\qquad \text{at}\quad x=0,$$
$$w(x,t)=0,\quad \frac{\partial^2 w(x,t)}{\partial x^2}=0,\qquad \text{at}\quad x=L. \tag{30}$$

Joule heating is produced when an electric current flows through a conductor and interacts with the moving particles that make up the current and the atomic ions that make up the conductor itself. When these particles, which make up the electrical current, collide with an ion, they lose some momentum. This kinetic energy causes the conductor's internal temperature to increase, which changes the electrical energy into thermal energy. When a potential voltage is applied across the first end of a microbeam ($x=0$), heat is generated with an intensity per volume of $E=I_e^2/\sigma_e$, where I_e is the current density described by I_{Th}/A, and σ_e is the electrical conductivity of the microbeam. The density of the current is considered to remain constant all along the microbeam. Due to the small scale of the investigation, it will be assumed that convection and thermal radiation from the microbeam are restricted and negligible. The average temperature along the portion of the microbeam caused by the current I_{Th} is governed by the following equation, which is derived using the heat equation (Fourier's law) and the aforementioned assumptions [14]:

$$-\frac{\partial \Theta(x,t)}{\partial x}=\frac{I_e^2}{\sigma_e}\qquad \text{at}\qquad x=0. \tag{31}$$

The electrothermal voltage V_e and current density may be expressed as $I_e=V_e\sigma_e/h$. Since this is the case, Equation (31) may be rewritten as [14]:

$$-\frac{\partial^2 \Theta(x,t)}{\partial x^2}=\frac{\sigma_e V_e^2}{h^2}\qquad \text{at}\qquad x=0. \tag{32}$$

In addition, it will be assumed that at the second terminal edge of the microbeam, the function $\Theta(x,t)$ satisfies the following condition

$$\frac{\partial \Theta}{\partial x}=0\qquad\qquad \text{at}\qquad x=L. \tag{33}$$

6. Laplace Transform Solution

The partial differential equation in the time domain may be transformed into a differential equation in the space domain with the help of a mathematical method known as the Laplace transform. After that, the result is transformed using the inverse Laplace operator on the response, which causes it to be translated back into the time domain. If $g(x,t)$ is a function that operates in the time domain, then the mathematical definition of its Laplace transform is given by:

$$\bar{g}(x,s)=\int_0^\infty g(x,t)\mathrm{e}^{-st}\mathrm{d}t. \tag{34}$$

Now, by taking the beginning conditions (29) and applying the Laplace transform to both sides of the basic equations given in (24)–(27), the following formulas can be obtained:

$$\left(\frac{\mathrm{d}^4}{\mathrm{d}x^4}-K_p\frac{\mathrm{d}^2}{\mathrm{d}x^2}+A_1\right)\bar{w}=-A_2\frac{\mathrm{d}^2\bar{\Theta}}{\mathrm{d}x^2} \tag{35}$$

$$-A_4\frac{\mathrm{d}^2\bar{w}}{\mathrm{d}x^2}=\frac{\mathrm{d}^2\bar{\Theta}}{\mathrm{d}x^2}-A_3\bar{\Theta}+A_7e^{-x/d} \tag{36}$$

$$\bar{M}=-A_5\bar{\Theta}-\frac{\mathrm{d}^2\bar{w}}{\mathrm{d}x^2} \tag{37}$$

$$\bar{\sigma}_x = -z\frac{\mathrm{d}^2\bar{w}}{\mathrm{d}x^2} - A_6\bar{\theta} \tag{38}$$

where

$$A_0 = \frac{12K_p}{h^2}, \quad A_1 = \frac{12s^2}{h^2} + K_v s + K_w, \quad A_2 = \frac{24\vartheta T_0\alpha_T}{k\pi^2 h}, \quad A_3 = \frac{\pi^2}{h^2} + \frac{s^2(1+s\tau_0)}{K_0 + \mathrm{s}},$$
$$A_5 = \frac{24\vartheta T_0\alpha_T}{k\pi^2 h}, A_4 = \frac{\alpha_T\pi^2 T_0^2 h\vartheta E(1+s\tau_0)}{24K(K_0+\mathrm{s})}, A_6 = T_0\alpha_T, A_7 = \frac{S_0(1+s\tau_0)}{K_0+s}, \tag{39}$$
$$K_0 = \frac{kK^*}{\vartheta^2 K}, \quad S_0 = \sqrt{\frac{4\ln(2)}{\pi}}\frac{\beta I_0(1-R)\pi^2 h^3 e^{2\beta}}{24dt_p(\beta + st_p)}.$$

Combining Equations (35) and (36) results in the differential equation shown below:

$$\left(\frac{\mathrm{d}^6}{\mathrm{d}x^6} - \eta_3\frac{\mathrm{d}^4}{\mathrm{d}x^4} + \eta_2\frac{\mathrm{d}^2}{\mathrm{d}x^2} - \eta_1\right)\bar{w}(x) = \phi_1 \mathrm{e}^{-x/d}, \tag{40}$$

where

$$\eta_3 = K_p + A_3 + A_2A_4, \quad \eta_2 = A_1 + K_pA_3, \qquad \eta_1 = A_1A_3, \phi_1 = \frac{A_2A_7}{d^2}. \tag{41}$$

It is possible to write the differential Equation (36) as follows:

$$\left(\frac{\mathrm{d}^4}{\mathrm{d}x^4} - m_1^2\right)\left(\frac{\mathrm{d}^4}{\mathrm{d}x^4} - m_2^2\right)\left(\frac{\mathrm{d}^4}{\mathrm{d}x^4} - m_3^2\right)\bar{w}(x) = \phi_1\mathrm{e}^{-x/d}, \tag{42}$$

where the roots of the equation:

$$m^6 - \eta_3 m^4 + \eta_2 m^2 - \eta_1 = 0, \tag{43}$$

are satisfied by the parameters $m_n^2,\ n = 1,2,3$.

The solution to Equation (52) can be expressed as follows:

$$\bar{w} = \textstyle\sum_{n=1}^{3}(\mathcal{P}_n\mathrm{e}^{-m_n x} + \mathcal{R}_n\mathrm{e}^{m_n x}) + \phi_2\mathrm{e}^{-x/d}, \tag{44}$$

where $\phi_2 = \frac{\phi_1 d^6}{1 - d^2\eta_3 + d^4\eta_2 - d^6\eta_1}$.

By using the conditions of the issue, it is possible to derive the values for the parameters $\mathcal{P}_n$ and $\mathcal{R}_n$, where $n = 1,2,3$ in Equation (44). Similarly, by removing the function $\bar{w}$ from Equations (35) and (36), the following equation can be arrived at:

$$\left(\frac{\mathrm{d}^4}{\mathrm{d}x^4} - m_1^2\right)\left(\frac{\mathrm{d}^4}{\mathrm{d}x^4} - m_2^2\right)\left(\frac{\mathrm{d}^4}{\mathrm{d}x^4} - m_3^2\right)\bar{\Theta}(x) = -\phi_3 e^{-x/d} \tag{45}$$

where $\phi_3 = \frac{A_7}{d^4}\left(1 - d^2K_p + d^4A_1\right)$.

It is possible to write the solution of Equation (45) as:

$$\bar{\Theta} = \textstyle\sum_{n=1}^{3}\mathcal{H}_n(\mathcal{P}_n\mathrm{e}^{-m_n x} + \mathcal{R}_n\mathrm{e}^{m_n x}) - \phi_4\mathrm{e}^{-x/d} \tag{46}$$

where:

$$\phi_4 = \frac{\phi_3 d^6}{1 - d^2\eta_3 + d^4\eta_2 - d^6\eta_1}, \quad \mathcal{H}_n = -\frac{m_n^4 - K_p m_n^2 + A_1}{m_n^2 A_2}. \tag{47}$$

With the assistance of Equations (44) and (46), one can construct the solution for the variables $\bar{M}$, $\bar{\sigma}_x$, and $\bar{u}$ in the Laplace domain as follows:

$$\bar{M}(x) = -\textstyle\sum_{n=1}^{3}(m_n^2 + A_5\mathcal{H}_n)(\mathcal{P}_n\mathrm{e}^{-m_n x} + \mathcal{R}_n\mathrm{e}^{m_n x}) + \left(\phi_4 A_5 - \frac{\phi_2}{d^2}\right)\mathrm{e}^{-x/d} \tag{48}$$

$$\bar{\sigma}_x = -\sum_{n=1}^{3}\left(z m_n^2 + A_6\,\mathcal{H}_n \sin\left(\frac{\pi z}{h}\right)\right)(\mathcal{P}_n e^{-m_n x} + \mathcal{R}_n e^{m_n x}) + \left(\phi_4 A_6 \sin\left(\frac{\pi z}{h}\right) - \frac{\phi_2}{d^2} z\right) e^{-x/d}, \tag{49}$$

$$\bar{u}(x) - z\frac{\partial \bar{w}}{\partial x} = \frac{\phi_2}{d} z e^{-x/d} + z\sum_{n=1}^{3} m_n(\mathcal{P}_n e^{-m_n x} - \mathcal{R}_n e^{m_n x}) \tag{50}$$

The boundary conditions (30) to (33) imposed on the problem can be transformed into the domain of the Laplace transform to become:

$$\begin{aligned} \bar{w}(0,s) &= 0, \quad \frac{\partial^2 \bar{w}(0,s)}{\partial x^2} = 0, \\ \bar{w}(L,s) &= 0, \quad \frac{\partial^2 \bar{w}(L,s)}{\partial x^2} = 0, \\ \frac{\partial \bar{\Theta}(0,t)}{\partial x} &= -\frac{\sigma_e V_e^2}{s h^2}, \quad \frac{\partial \bar{\Theta}(L,s)}{\partial x} = 0. \end{aligned} \tag{51}$$

Boundary conditions (49) are inserted with Equations (40) and (42) to yield:

$$\sum_{n=1}^{3}(\mathcal{P}_n + \mathcal{R}_n) = -\phi_{2,} \tag{52}$$

$$\sum_{n=1}^{3} m_n^2(\mathcal{P}_n + \mathcal{R}_n) = -\frac{\phi_2}{d^2}, \tag{53}$$

$$\sum_{n=1}^{3}(\mathcal{P}_n e^{-m_n L} + \mathcal{R}_n e^{m_n L}) = -\phi_2 e^{-L/d} \tag{54}$$

$$\bar{w} = \sum_{n=1}^{3} m_n^2(\mathcal{P}_n e^{-m_n L} + \mathcal{R}_n e^{m_n L}) = -\frac{\phi_2}{d^2} e^{-L/d} \tag{55}$$

$$\sum_{n=1}^{3} m_n \mathcal{H}_n(\mathcal{P}_n + \mathcal{R}_n) = -\frac{\phi_4}{d} - \frac{\sigma_e V_e^2}{s h^2} \tag{56}$$

$$\sum_{n=1}^{3} m_n \mathcal{H}_n(\mathcal{P}_n e^{-m_n L} + \mathcal{R}_n e^{m_n L}) = -\frac{\phi_4}{d} e^{-\frac{L}{d}} \tag{57}$$

By solving this system of linear equation, the values of the two unknown parameters $\mathcal{P}_n$ and $\mathcal{R}_n$, where $n = 1,2,3,$ can be determined.

7. Numerical Inversion Technique

The Laplace transform inversion issue on the real axis is an ancient and challenging numerical inversion problem. This topic has been the subject of several academic studies and represents a significant issue in scientific computing. This ill-posed inverse issue can be solved in several ways [40–43].

In this study, a straightforward formula for calculating the inverse Laplace transform for real-world data will be presented without resorting to standard regularization techniques.

The Gaver–Stehfest technique, given in [44] and [45], is one of the most often used inversion algorithms, particularly in reservoir engineering, where it is essential for the Laplace argument s to be real ($s \in \Re$). Most of the time, this approach produces acceptable results, mainly when used to smooth functions. The Gaver–Stehfest method relies on the following approximation [46]:

$$f(x,t) = \frac{ln(2)}{t}\sum_{i=1}^{M} a_i \bar{F}\left(x, i\frac{ln(2)}{t}\right), \quad M = 2n, \ n \geq 1, t > 0, \tag{58}$$

in which the parameters a_i are provided as follows:

$$a_i = (-1)^{n+k}\sum_{j=\frac{k+1}{2}}^{\min(k,n)} \frac{j^n(2j)!}{(n-j)!\,j!\,(j-1)!\,(k-j)!\,(2j-k)!}. \tag{59}$$

The parameter $M = 2n$, sometimes called the "Stehfest number", must be an even integer. Since the weighting coefficients a_i depend only on the Stehfest number M, they may be computed once during a pre-processing phase. Various other considerations of microstructured media can be found in [47–50].

8. Numerical Results and Analysis

To depict the thermo-dynamic behavior of the thin microbeam on the viscous Pasternak basis with a heat supply in the form of laser pulses, an analytical and numerical solution was derived in the preceding sections, taking into consideration the thermoelectric influence. In the present section, the analytical results obtained from the literature will be reviewed, and the effects of several essential elements and parameters on the variations of the considered field variables, such as nondimensional temperature and deflection, will be examined. The current approach suffers from a lack of actual empirical cases, which can be used to measure the physical domains being investigated and then compare them to others.

As far as the authors are aware, there has been no previous research into the thermo-mechanical consequences of analyzing vibration in a thermoelectric beam using the generalized theory of thermoelasticity. For this reason, the present article uses general thermoplastic models to consider the vibrational properties of a microbial beam based on a viscoelastic-Pasternak base. To determine how to solve this problem, relevant theoretical issues will be considered, along with how the results are similar and different. Here, the numerical findings of a silicon-doped microbeam will be presented, considering the physical parameters listed in Table 1.

Table 1. Physical values of the doped silicon microbeam.

Quantity	Symbol	Value
Density	ρ	2332 (kg/m^3)
Young's Modulus	E	120 GPa
Length	L	600 μm
Width	b	20 μm
Thickness	h	10 μm
Thermal expansion coefficient	α_t	2.59×10^{-6} (1/K)
Thermal conductivity	K	165 W/(m K)
Specific heat	C_E	130 J/(kg K)
Electrical conductivity	σ_e	0.78×10^4 (S/m)
Poisson's ratio	ν	0.22
Laser intensity	I_0	13.4 (W/m^2)
Laser penetration depth	d	15.3×10^{-9} m
Constant parameter	β	1.992
Ambient temperature	T_0	300 K
Laser pulse duration	t_p	100×10^{-15} s
Relaxation time	τ_0	8.5×10^{-12} s
Surface reflectivity	R	0.93

Due to the application of non-dimensional values in the problem, it will be assumed that $L = 1$ and $z = h/3$ in the numerical calculations. The results are graphically shown in Figures 2–11 and Table 2, with values ranging from 0 to 1.0 at different x-coordinates. Based on the analytical solutions obtained previously, numerous numerical examples were presented to study how the visco-foundation Pasternak indices (shear stiffness K_p, damping modulus of the foundation K_v, and horizontal spring stiffness K_w) affect the beam response under the influence of the thermoelectric heat flow. Simulation results are also used to look at how the rise time of the laser t_p and the electrothermal voltage coefficient V_e affect the temperature of the microbeam and how it bends. This is completed to better understand the thermoelectric phenomena.

8.1. The Influence of Visco-Pasternak's Basis Factors

In this subsection, the numerical results of the different field variables for studying the vibration of thermoelectric microbeams and evaluating their temperature θ, deformation u, and deflection w will be presented, taking into account the changes in the non-dimensional visco-Pasternak flexible basis factors (K_p, K_w, and K_v). Table 2 shows how the coefficients K_p, K_w, and K_v affect the thermomechanical properties of the microbeam. The researchers used a modified version of the MGT heat transfer equation so that they could study the different variations and give facts and figures for each. In order to make comparisons, the non-dimensional values $K^* = 200$, $t_p = 0.01$, $\tau_0 = 0.03$, $V_e = 10$, and $t = 0.12$ can be set. It can be seen that the results can be obtained from comprehensive thermoplastic calculations for beams without a visco-Pasternak elastic basis by setting $K_p = K_w = K_v = 0$.

The numerical data in Table 2 illustrates the influence of the Pasternak parameter (shear stiffness) K_p on the values of various domains as a function of distance. One can see that as the shear stiffness K_p increases, so do the values of the deflection w in this table. The numerical data show that increasing the constant base factors mitigates the effects of the Winkler and Pasternak coefficients K_w and K_p on the deflection w. This is because a more rigid microbeam system is inherently stronger. Table 2 displays the relationship between deflection and the Winkler stiffness modulus K_w. Moreover, in Table 2, the studied domains are represented against the distance for a variety of viscous damping coefficient values (K_v). As the damping coefficient K_v rises, the physical fields become increasingly noticeable. This is expected due to the fact that linear deviation is proportional to K_v.

The table shows that the absolute values of the nondimensional thermal stress σ_x, as well as the bending moment M, increased with the increase in the Winkler stiffness parameter (K_w) and Pasternak (K_p) coefficients. The precision girder stability is enhanced as a result of the increased structural rigidity in K_w and K_p. Changes in the visco-Pasternak basis profoundly affect the bending moment M and the deflection within the microbeam. Variations in the coefficients of the Pasternak viscous basis have less effect on the deformation u and temperature θ.

Table 2. The influence of visco-Pasternak parameters K_p, K_w, and K_v on the studied fields.

K_v	K_w	K_p	Thermo-Physical Fields				
			w	θ	u	σ_x	M
0.2	0.0	0.0	−0.0609143	2.85630	0.101218	−0.564227	−0.406249
	0.1	0.2	−0.0597582	2.85663	0.101314	−0.558596	−0.406141
	0.2	0.3	−0.0591818	2.85680	0.101359	−0.555789	−0.405988
	0.3	0.4	−0.0586066	2.85696	0.101402	−0.552988	−0.405758
0.4	0.0	0.0	−0.0608022	2.85631	0.101190	−0.563906	−0.406248
	0.1	0.2	−0.0601662	2.85649	0.101243	−0.560807	−0.406133
	0.2	0.3	−0.0590141	2.85682	0.101335	−0.555195	−0.405971
	0.3	0.4	−0.0584398	2.85699	0.101378	−0.552398	−0.405727
0.6	0.0	0.0	−0.060650	2.85632	0.101152	−0.563469	−0.406246
	0.1	0.2	−0.059497	2.85665	0.101247	−0.557849	−0.406136
	0.2	0.3	−0.0589221	2.85682	0.101291	−0.555049	−0.405982
	0.3	0.4	−0.0583485	2.85698	0.101334	−0.552255	−0.405750
0.8	0.0	0.0	−0.0604983	2.85633	0.101114	−0.563033	−0.406244
	0.1	0.2	−0.0593470	2.85667	0.101208	−0.557421	−0.406133
	0.2	0.3	−0.0587731	2.85683	0.101252	−0.554624	−0.405978
	0.3	0.4	−0.0582004	2.85700	0.101295	−0.551833	−0.405747

It is seen from the numerical values in the table that the quantities of the different thermophysical fields decline when the Winkler and Pasternak coefficients K_w and K_p remain unchanged with the increase in the viscous damping coefficient K_v. In addition, when there is a change in the viscous damping parameter K_v, there is little variation in the temperature and displacement values. The absolute value of the deviation w increases as the viscosity parameter K_v decreases. As the viscous damping modulus K_v and other exponents are increased, the dimensionless axial stress σ_x and flexure moment M increase.

It has been observed that increasing the viscoelastic structural damping parameter K_v of microscale beams can reduce the internal thermophysical fields. The reason for this is that a rise in the structural damping coefficient K_v causes the structure to be less rigid. The influence of the viscous structural damping parameter is more pronounced when the Winkler and Pasternak parameters K_w and K_p remain unchanged. This review article can provide useful information for the design of some fine structural systems by helping to choose the appropriate foundation model, which must take into account the stability, control, and vibrations of the structural system being treated or designed. As a consequence of the analysis mentioned above, it is clear that the anticipated results will be on the low side for the problem if shear stiffness, damping, or transverse impact are ignored. Engineering that considers these factors will produce better results at a lower cost.

8.2. Effect of Laser Pulse Duration t_p

This present work studied the transient electrical and thermal conductivity in thin silicon bundles subjected to short-pulse laser heating as a heat source by means of the MGT thermal conductivity model. Exciting the metal with an ultrafast laser can cause the material to enter a state very different from its original equilibrium. A system of cold, highly bound ions immersed in a partially degenerated electron sea is produced due to the preferential and rapid heating of one subsystem compared to another. These temporary states frequently occur during the formation of high-energy-density plasmas, which can contain warm, dense matter. These cases are particularly relevant for laser micromachine fusion studies and self-entrapment fusion studies because of their transient nature. In the laboratory, these short-lived states are used to test quantum mechanics theories of nuclear dynamics, electron-ion interactions, and phase transitions.

It is very important to study the thermal influence that a non-Gaussian laser has on thermoelastic microbeams when using a laser as a heat source using modified heat transfer models. In this subsection, the heating of microbeams using a pulsed laser as a heating source will be investigated. The microbeam is made of silicon and is heated by a pulsed non-Gaussian laser beam with a duration t_p. The interaction between temperature change and stress dissipates energy, converting temporary mechanical energy into more stable thermal energy within the material. Figures 2–5 show the numerical values of the different fields for the purpose of investigating how the laser pulse length t_p affects the relationship between the dimensionless temperature and the amount of deflection and deformation that occurs inside the microbeam. All other influencing factors involving K_p, K_w, K_v, τ_0, and K^* remain constant in the numerical calculations.

When the solid microbeam is exposed to pulsed laser light on its surface, the material inside begins to vibrate in the form of waves. As shown in Figures 2 and 4, thermoelastic waves are formed by thermal expansion near the surface during pulsed laser heating and are transmitted to the microbeam, which leads to increased deformation and deflection.

Due to the short length of the laser pulse, the heating process will be extremely fast, making the Fourier transfer theory invalid, as it predicts infinite velocities for heat waves. For this reason, a modified non-Fourier heat transfer equation (MGT model) was used in the present work, considering that thermal signals can only travel at a finite speed within the medium. These results demonstrate that the MGTE model shows excellent practical and theoretical consistency for mechanical properties.

Increases in the laser pulse length increase the temperature and the intermolecular distances between the beam materials, while simultaneously reducing the intermolecular thrust. As the duration of the laser pulse increases, the temperature decreases within the microbeam, which stands on the viscoelastic Pasternak foundation (see Figure 3). This is because the structural pieces are moved at such a high rate by an ultrashort laser pulse that the resulting inertial forces are so great that the structure vibrates more than usual. One thing to keep in mind is that in the laser process, thermoelasticity and momentum coexist and can have an effect on each other, although these two phenomena are rarely studied together.

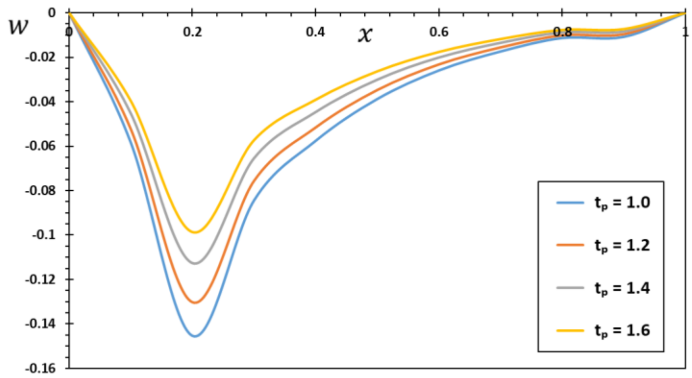

Figure 2. The deflection w versus several durations of the laser pulse t_p.

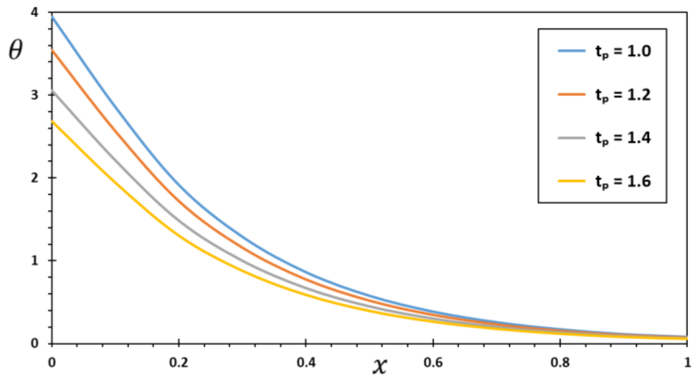

Figure 3. The temperature θ versus several durations of the laser pulse t_p.

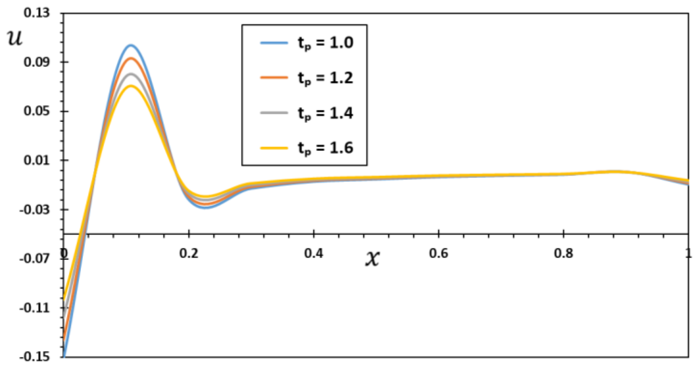

Figure 4. The axial displacement u versus several durations of the laser pulse t_p.

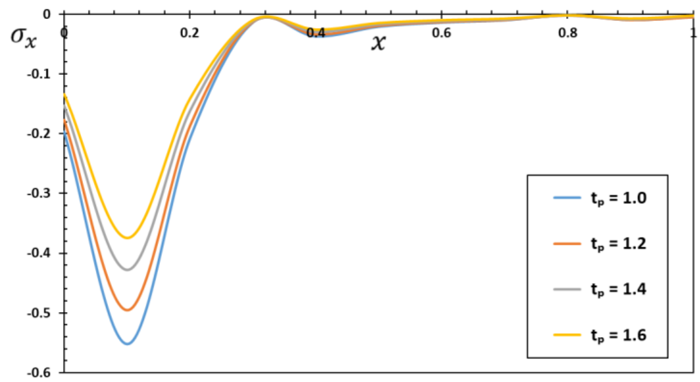

Figure 5. The thermal stress σ_{xx} versus several durations of the laser pulse t_p.

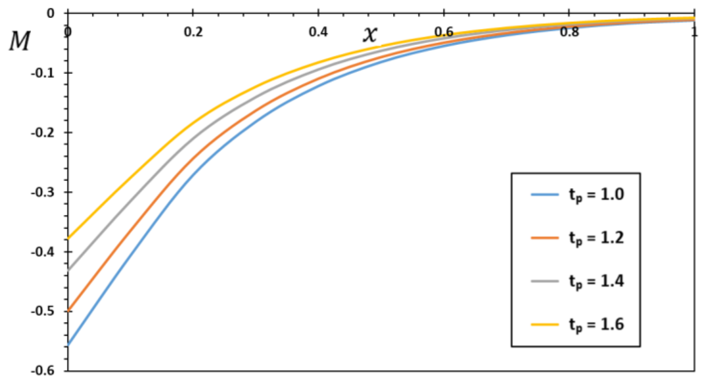

Figure 6. The bending moment M versus several durations of the laser pulse t_p.

8.3. The Effect of Electrothermal Voltage

The thermoelectric microbeam that is the subject of this investigation is given a thermal load through electrothermal operation by having an external circuit added to the first edge of the beam. In the micro-structures and machinery industry, thermoelectric activation is often used to excite and tune harmonic resonators. Thermally tuned micro/nanoelectromechanical and electromechanical devices are useful for many applications, such as communication systems, process filtration, systems with gyroscopes, power control, and sensitivity detection. The fluctuations of beam deflection and other investigated thermomechanical fields are expressed in Figures 7–11 as a response to the applied thermoelectric load (voltages V_e). In this case, the microspheres would be electrically excited by applying different values of the thermoelectric voltages, $V_e = 10$ V, $V_e = 20$ V, $V_e = 30$ V, and $V_e = 40$ V. At the same time, the other influencing constants will be assumed to be constant.

From Figure 7, it is interesting to note that the amount of deflection increases with increasing electrical voltages. This is due to the increase in the thermal and electrical load (electrothermal voltage) produced inside the microbeam. It is well known that its temperature increases as current travels through a conductor. Collisions between moving electrons and the conductor's atoms cause the electrons to lose some of their energy, which is then transformed into heat when the electrons pass through the conductor. As a result, the conductor's temperature rises. Figure 8 shows the significant effect of voltage on the temperature distribution. With the increase in the amount of voltage in the electrical circuit from the first end of the microbeam, the thermal load increases, leading to an increase in temperature. Temperature differences decrease as one moves away from the source of the electric heat flow. Figure 9 shows that the compressive stress inside the microbeams increases when the ferroelectric voltage rises. This causes the microbeams to buckle and the bending moment to increase. From Figure 9, it can be expected that the shape of the microbeams will change near the thermoelectric load at the beginning of the microbeam. This is because the microbeam is subjected to a compressive force that increases as the thermoelectric potential increases.

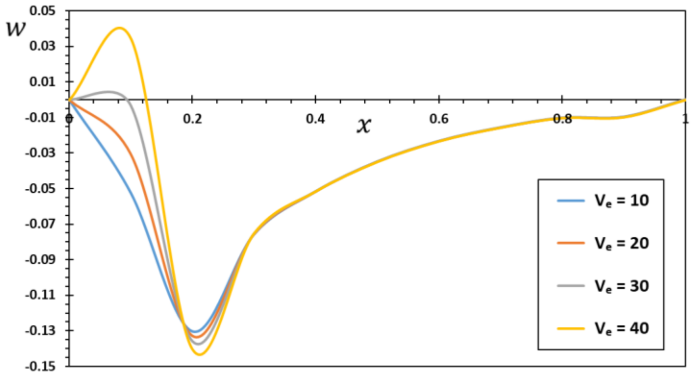

Figure 7. The thermal deflection w versus various electrothermal voltages V_e.

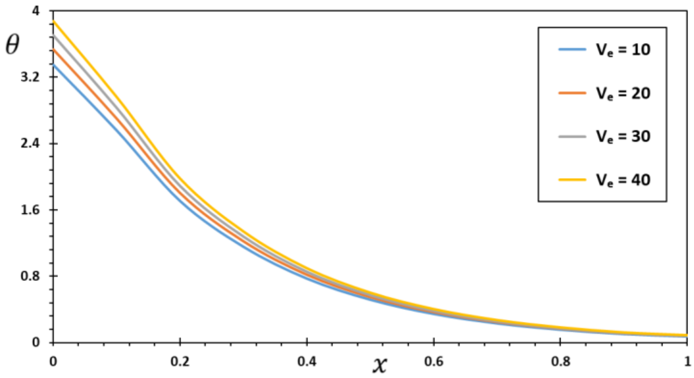

Figure 8. The temperature θ versus various electrothermal voltages V_e.

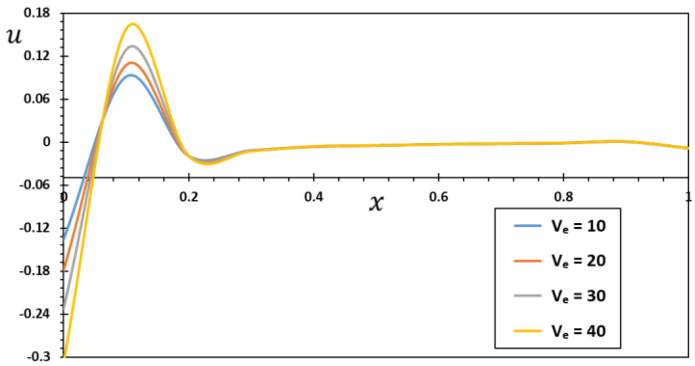

Figure 9. The displacement u versus various electrothermal voltages V_e.

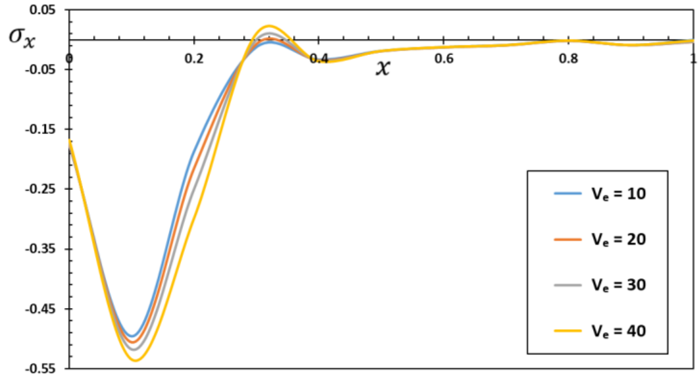

Figure 10. The thermal stress σ_x versus various electrothermal voltages V_e.

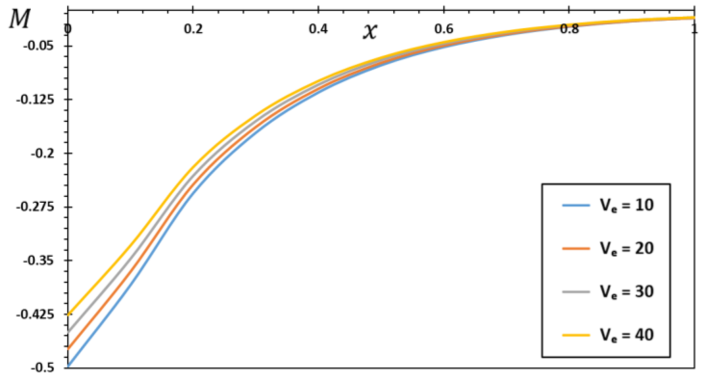

Figure 11. The bending moment M versus various electrothermal voltages V_e.

9. Conclusions

In this paper, a mathematical model is given to study the thermoelastic vibrational behavior of thin microbeam that are embedded in a three-parameter viscoelastic foundation. The thermal interactions between a microbeam and a viscoelastic foundation were simulated using the Winkler–Pasternak elastic foundation model. In addition, a new heat transfer model incorporating the Moore–Gibson–Thompson formula is introduced. The microbeam undergoes a heating effect when electrical current and voltage are applied through a graphene sheet. Moreover, it is exposed to laser heating pulses as an internal heat source with changing properties over time. The effects of the three different foundation parameters, ferroelectric voltage, and laser pulse duration coefficient were shown. From the discussions and analysis, the following conclusions can be drawn:

- The results show that increasing the Winkler and foundation shear moduli reduces microbeam deflection and first-side axial deformations. This reduction is a direct consequence of the higher beam stiffness. However, as the viscosity index is raised, the deflection and deformation significantly increase.
- As Pasternak's modulus and Winkler's viscosity factor increase, flexural moment and axial stress also increase. Increasing the coefficient of the visco-Pasternak base reduces the dynamic behavior of the microbeam, facilitating a much faster attempt at equilibrium. Increasing the viscous damping coefficients results in a significant decrease in the amplitudes of the studied work areas and the response time.
- Theoretical analysis and experimental results showed that a solid base is necessary for the stability of the building when it is in a state of oscillation. Every building needs a solid foundation on which to rest, as this helps prevent any kind of mechanical failure from occurring.
- The results show that the MGTE model has a good theoretical and experimental agreement between the mechanical properties and the physical aspects.

- The magnitudes of deflection increase with increasing electrical voltages. This is due to the increase in the thermos-electrical load (electrothermal voltage) produced inside the microbeam.

Author Contributions: Conceptualization, all authors; methodology, A.E.A. and M.M.; validation and investigation, A.E.A.; writing—original draft preparation, A.E.A. and M.M.; writing—review and editing, A.E.A. and S.S.A.; visualization, A.E.A., M.M., and S.S.A.; supervision, S.S.A. All authors have read and agreed to the published version of the manuscript.

Funding: This project is funded by King Saud University, Riyadh, Saudi Arabia.

Data Availability Statement: Not Applicable.

Acknowledgments: This research is supported by project number (RSP2023R167), King Saud University, Riyadh, Saudi Arabia.

Conflicts of Interest: The authors declare no conflict of interest. The authors affirm that they are not aware of any financial or interpersonal conflicts that might have affected the work reported in this publication.

References

1. Zenkour, A.M.; Abouelregal, A.E. Effect of harmonically varying heat on FG nanobeams in the context of a nonlocal two-temperature thermoelasticity theory. *Euro. J. Comp. Mech.*, **2014**, 23, 1–14.
2. Craighead, H.G. Nanoelectromechanical Systems. *Science* **2000**, *290*, 1532–1535.
3. Li, C.; Zhu, C.X.; Lim, C.W.; Li, S. Nonlinear in-plane thermal buckling of rotationally restrained functionally graded carbon nanotube reinforced composite shallow arches under uniform radial loading. *Appl. Math. Mech.* **2022**, *43*, 1821–1840.
4. LI, C. Size-dependent thermal behaviors of axially traveling nanobeams based on a strain gradient theory. *Struc. Eng. Mech.* **2013**, *48*, 415–434.
5. Li, C.; Zhu, C.X.; Zhang, N.; Sui, S.H.; Zhao, J.B. Free vibration of self-powered nanoribbons subjected to thermal-mechanical-electrical fields based on a nonlocal strain gradient theory. *Appl. Math. Model.* **2022**, *110*, 583–602.
6. Sui, S.; Zhu, C.; Li, C.; Lei, Z. Free Vibration of Axially Traveling Moderately Thick FG Plates Resting on Elastic Foundations. *J. Vib. Eng. Technol.* **2023**, *11*, 329–341.
7. Zemskov, A.; Hao, L.; Tarlakovskii, D. Bernoulli-Euler beam unsteady bending model with consideration of heat and mass transfer. *J. Appl. Comp. Mech.* **2023**, *9*, 168–180.
8. Ashraf, M.W.; Tayyaba, S.; Afzulpurkar, N. Micro electromechanical systems (MEMS) based microfluidic devices for biomedical applications. *Int. J. Mol. Sci.* **2011**, *12*, 3648–3704.
9. Shi, D.; Zhang, H.; Wang, Q.; Zha, S. Free and forced vibration of the moderately thick laminated composite rectangular plate on various elastic Winkler and Pasternak foundations. *Shock Vibr.* **2017**, *2017*, 7820130.
10. Zemskov, A.V.; Tarlakovskii, D.V. Unsteady elastic diffusion bending model for a Timoshenko beam on a Winkler foundation. *Arch. Appl. Mech.* **2022**, *92*, 1355–1366.
11. Zemskov, A.V.; Okonechnikov, A.S.; Tarlakovskii, D.V. Unsteady Elastic–Diffusion Vibrations of a Simply Supported Euler–Bernoulli Beam Under the Distributed Transverse Load. In *Multiscale Solid Mechanics. Advanced Structured Materials*; Altenbach, H., Eremeyev, V.A., Igumnov, L.A., Eds.; Springer: Cham, Switzerland, 2021; Volume 141.
12. Togun, N.; Bağdatli, S.M. The vibration of nanobeam resting on elastic foundation using modified couple stress theory. *Teh. Glas.* **2018**, *12*, 221–225.
13. Saadatnia, Z.; Askari, H.; Esmailzadeh, E. Multi-frequency excitation of microbeams supported by Winkler and Pasternak foundations. *J. Vibr. Control* **2017**, *24*, 2894–2911.
14. Hajjaj, A.Z.; Alcheikh, N.; Ramini, A.; Al Hafiz, M.A.; Younis, M.I. Highly Tunable Electrothermally and Electrostatically Actuated Resonators. *J. Microelectromechanical Syst.* **2016**, *25*, 440–449.
15. Liu, Y.; Zhou, S.; Wu, K.; Qi, L. Size-dependent electromechanical responses of a bilayer piezoelectric microbeam. *Int. J. Mech. Mater. Design.* **2020**, *16*, 443–460.
16. Pimpare, S.B.; Sutar, C.S. Hollow cylinder with thermoelastic modelling by reduced differential transform. *J. Indones. Math. Soc.* **2022**, *28*, 8–18.
17. Biot, M. Thermoelsticity and Irreversible Thermodynamics. *J. Appl. Phys.* **1956**, *27*, 240–253.
18. Lord, H.; Shulman, Y. A generalized dynamic theory of thermoelasticity. *J. Mech. Phys. Solids* **1967**, *15*, 299–309.
19. Green, A.E.; Lindsay, K.A. Thermoelasticity. *J. Elast.* **1972**, *2*, 1–7.
20. Green, A.E.; Naghdi, P.M. A re-examination of the basic postulates of thermomechanics. *Proc. R. Soc. Lond. Ser. A* **1991**, *432*, 171–194.
21. Green, A.E.; Naghdi, P.M. On undamped heat waves in an elastic solid. *J. Therm. Stress.* **1992**, *15*, 253–264.
22. Green, A.E.; Naghdi, P.M. Thermoelasticity without energy dissipation. *J. Elast.* **1993**, *31*, 189–208.
23. Quintanilla, R. Moore–Gibson–Thompson thermoelasticity. *Math. Mech. Solids.* **2019**, *24*, 4020–4031.

24. Quintanilla, R. Moore-Gibson-Thompson thermoelasticity with two temperatures. *Appl. Eng. Sci.* **2020**, *1*, 100006.
25. Abouelregal, A.E.; Sedighi, H.M.; Eremeyev, V.A. Thermomagnetic behavior of a semiconductor material heated by pulsed excitation based on the fourth-order MGT photothermal model. *Continuum Mech. Thermodyn.* **2023**, *35*, 81–102.
26. Abouelregal, A.E.; Rayan, A.; Mostafa, D.M. Transient responses to an infinite solid with a spherical cavity according to the MGT thermo-diffusion model with fractional derivatives without nonsingular kernels. *Waves Random Complex Media* **2022**. https://doi.org/10.1080/17455030.2022.2147242
27. Moaaz, O.; Abouelregal, A.E.; Alsharari, F. Analysis of a transversely isotropic annular circular cylinder immersed in a magnetic field using the Moore–Gibson–Thompson thermoelastic model and generalized Ohm's law. *Mathematics* **2022**, *10*, 3816.
28. Conti, M.; Pata, V.; Quintanilla, R. Thermoelasticity of Moore–Gibson–Thompson type with history dependence in the temperature. *Asymptot. Anal.* **2020**, *120*, 1–21.
29. Gupta, S.; Dutta, R.; Das, S.; Pandit, D.K. Hall current effect in double poro-thermoelastic material with fractional-order Moore–Gibson–Thompson heat equation subjected to Eringen's nonlocal theory. *Waves Random Complex Media* **2022**. https://doi.org/10.1080/17455030.2021.2021315
30. Marin, M. On existence and uniqueness in thermoelasticity of micropolar bodies, Comptes rendus de l'Académie des Sciences Paris. *Série II B* **1995**, *321*, 375–480.
31. Marin, M.; Marinescu, C. Thermoelasticity of initially stressed bodies. Asymptotic equipartition of energies. *Int. J. Eng. Sci.* **1998**, *36*, 73–86.
32. Hetényi, M. *Beams on Elastic Foundation: Theory with Applications in the Fields of Civil and Mechanical Engineering*; University of Michigan: Ann Arbor, MI, USA, 1971.
33. Younesian, D.; Hosseinkhani, A.; Askari, H.; Esmailzadeh, E. Elastic and viscoelastic foundations: a review on linear and non-linear vibration modeling and applications. *Nonlinear Dyn.* **2019**, *97*, 853–895.
34. Miao, Y.; He, H.; Yang, Q.; Shi, Y. Analytical solution considering the tangential effect for an infinite beam on a viscoelastic Pasternak foundation. *Appl. Math. Model.* **2020**, *85*, 231–243.
35. Demir, C.; Civalek, Ö. On the analysis of microbeams. *Int. J. Eng. Sci.* **2017**, *121*, 14–33.
36. Darban, H.; Fabbrocino, F.; Feo, L.; Luciano, R. Size-dependent buckling analysis of nanobeams resting on two-parameter elastic foundation through stress-driven nonlocal elasticity model. *Mech. Adv. Mater. Struct.* **2021**, *28*, 2408–2416
37. Younesian, D.; Kargarnovin, M.H. Response of the beams on random Pasternak foundations subjected to harmonic moving loads. *J Mech Sci Technol* **2009**, *23*, 3013–3023.
38. Ramadan, K.; Tyfour, W.R.; Al-Nimr, M.A. On the analysis of short-pulse laser heating of metals using the dual phase lag heat conduction model. ASME J. *Heat Transf.* **2009**, *131*, 111301.
39. Lee, H.-L.; Chen, W.-L.; Chang, W.-J.; Yang, Y.-C. Estimation of energy absorption rate and temperature distributions in short-pulse laser heating of metals with a dual-phase-lag model. *Appl. Therm. Eng.* **2014**, *65*, 352–360.
40. Campos, R.G.; Huet, A. Numerical inversion of the Laplace transform and its application to fractional diffusion. *Appl. Math. Comput.* **2018**, *327*, 70–78.
41. Davies, B.; Martin, B. Numerical inversion of the Laplace transform: a survey and comparison of methods. *J. Comput. Phys.* **1979**, *33*, 1–32.
42. Gzyl, H.; Tagliani, A.; Milev, M. Laplace transform inversion on the real line is truly ill-conditioned, Appl. *Math. Comput.* **2013**, *219*, 9805–9809.
43. Honig, G.; Hirdes, U. A method for the numerical inversion of Laplace transforms. *J. Comput. Appl. Math.* **1984**, *10*, 113–132.
44. Stehfest, H. *Algorithm* 368: Numerical inversion of Laplace transforms [D5]. *Commun. ACM* **1970**, *13*, 47–49.
45. Stehfest, H. Remark on algorithm 368: Numerical inversion of Laplace transforms. *Commun. ACM* **1970**, *13*, 624.
46. Wójcik, M.; Szukiewicz, M.; Kowalik, P. Application of Numerical Laplace Inversion Methods in Chemical Engineering with Maple®. *J. Appl. Comput. Sci. Methods* **2015**, *7*, 5–15.
47. Marin, M.; Öchsner, A. The effect of a dipolar structure on the Hölder stability in Green–Naghdi thermoelasticity, Contin. *Mech. Thermodyn.* **2017**, *29*, 1365–1374.
48. Luminiţa, S.M.; Sorin, V.; Marin, M.; Arina, M. New analytical method based on dynamic response of planar mechanical elastic systems. *Bound. Val. Probl.* **2020**, *2020*, 104.
49. Abouelregal, A.E.; Marin, M. The response of nanobeams with temperature-dependent properties using state-space method via modified couple stress theory. *Symmetry* **2020**, *12*, 1276.
50. Marin, M.; Ellahi, R.; Vlase, S.; Bhatti, M.M. On the decay of exponential type for the solutions in a dipolar elastic body. *J. Taibah Univ. Sci.* **2020**, *14*, 534–540.